Motor-induced sliding of microtubule and actin bundles

Assaf Zemel[ab] **and Alex Mogilner**[*a]

Interactions of multiple molecular motors with bundles of actin and microtubule filaments form the basis for many cytoskeletal processes including axonal growth, muscle contraction, cell division and platelet formation. Continuum models based on generalized diffusion equations have been suggested to quantify the dynamics of such active bundles. In highly cross-linked and densely packed filament bundles, however, a major complication arises due to the multiple interactions that each filament forms with its neighbors. To explore the effects of these interactions, we used detailed computer simulations and studied the bundles with different types of motors at different densities and boundary conditions. We found that highly cross-linked bundles exhibit effects of long-ranged interactions that are sensitive to the boundary conditions. In open bundles, these give rise to 'telescopic' patterns resulting in significant acceleration of the filaments at the edges. In contrast, in ringed bundles, the long-ranged interactions 'lock' filaments and slow down their movements. The filaments in loosely connected bundles, on the other hand, undergo local diffusion-drift dynamics consistent with previous continuum models. Our simulations also demonstrate the sorting phenomena in the mixed-polarity bundles and reveal characteristic scales and conditions for spontaneous pattern formation in the bundle. We discuss the relevance of our results for cytoskeleton systems such as microtubules in axons, platelet formation, kinetochore fibers and actin bundles in motile cells.

1. Introduction

The cytoskeleton-intracellular scaffold-largely consists of microtubules and actin filaments providing lines of transport and communication in the cell and organizing cell movements and division.[1] Polarity of the cytoskeletal filaments (their distinctive minus and plus ends) dictates the direction of motion of the molecular motors. Each motor always 'walks' toward the same end of the filament, *i.e.* dynein-toward microtubule minus end, kinesin-1-toward microtubule plus end, *etc.* The molecular motors are often deployed to transport vesicles and organelles, as well as to generate forces, in addition to their participation in self-organization of the cytoskeletal structures in the cell.[2] In some of these processes, the motors cross-link neighboring filaments and slide them with respect to each other, as well as deform the filaments and alter their dynamics.[3]

Some of the filament-motor structures, such as mitotic spindle and lamella, are highly complex and multi-dimensional, while others have a simpler architecture and are more amenable to theoretical modeling. Here we examine the sliding dynamics of one-dimensional, microtubule or actin bundles (Fig. 1). There are multiple examples of the microtubule bundles in cells.[4,5] Of particular interest are the microtubule bundles that power formation of blood platelets from megakaryocytes in bone marrow.[6] When the megakaryocyte reaches maturation, protrusions that consist of dense bundles

[a] *Department of Neurobiology, Physiology and Behavior, University of California, Davis, USA. E-mail: mogilner@math.ucdavis.edu*
[b] *Institute of Dental Sciences, Hebrew University of Jerusalem, Hadassah Medical Center, Jerusalem, Israel*

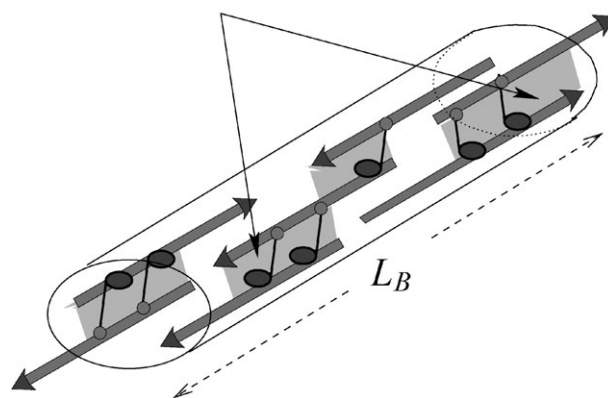**Fig. 1** Schematic illustration of a cross-linked microtubule bundle. L_B is the bundle length and L is the length of each filament. The arrow of each filament shows the gliding direction of the motor protein on the filament; for example, for a minus-end directed motor (*i.e.* dynein) the arrow points in the minus-end direction of the filament. M is the total number of potential overlaps between pairs of filaments in the bundle, and M_b is the number of overlaps that are cross-bridged by the motors (shadowed in the figure); $\chi_b = M_b/M$ is the fraction of active overlaps is the bundle. In Fig. 1–3, binding domains at the motors' ends are marked with the small disc, while the motor (moving) domains-with the ellipse.

of microtubules enveloped by cell membrane are formed; these bundles, in which hundreds of filaments are cross-linked by dynein motors, expand to form elongated proplatelet shafts that eventually branch, taper and break into thousands of

newly formed platelets. There is also a growing body of evidence that similar microtubule-motor expansion is responsible for growth and maintenance of axons,[7] neurites[8,9] and nerve growth-cones.[10]

More complex microtubule-motor bundles are found in the mitotic spindle of dividing cells.[11] In the so-called inter-polar bundles, microtubules of opposite polarity overlap at the spindle 'equator' where kinesin-5 motors slide the microtubules apart, thereby elongating the spindle.[12] Kinesin-5 motor is bipolar, namely, it has motor domains on both ends, so rather than binding a filament at one end and sliding another filament with the motor domain at the other end, kinesin-5 symmetrically uses two motor domains to slide both filaments the motor is in contact with.[13] The mitotic spindle consists of many short microtubules[14] densely crosslinked by various motors, rather than of long filaments that span the entire length of the bundle. These cross-linked microtubules can slide on one another in a 'piggy-backing' fashion.[15]

Actin filaments also organize into the bundles cross-linked by myosin motors and other bundling proteins. Most notable examples of such bundles are muscle sarcomere and stress-fiber of an adherent cell.[16,17] Less organized contractile actin-myosin bundles are observed across the motile appendages of rapidly migrating cells.[18] Another ubiquitous and dynamic acto-myosin bundle is the contractile ring of dividing cells,[19–21] in which the actin-myosin bundle has periodic boundary conditions.

In this paper, we do not focus on a particular biological process but rather investigate physical properties of the filament-motor bundles. A number of elegant models have been suggested for this purpose.[12,15,19–26] Many of these models, however, are limited to dilute concentrations of motors and to local pairwise interactions between the filaments. Here we use detailed computer simulations to examine both low and high motor concentrations and to explicitly account for the effects of high connectivity of the filaments in the bundle. Our simulations predict several interesting phenomena in the dynamic self-organizing filament-motor bundles. We observe a marked difference in the dynamics of loosely and highly interconnected bundles— the latter form long-ranged interactions between the filaments that can span the entire length of the bundle. This results in a strong effect of the boundary conditions on the motion of the filaments. In free and open bundles, 'telescopic' patterns form that cause substantial acceleration of the filaments at the bundle's ends. In contrast, in ringed bundles, the long-ranged motor-induced interactions between the filaments result in significant slowing down: the motors act as brakes to the filament sliding. Loosely connected bundles, on the other hand, exhibit local diffusion-drift dynamics consistent with previous continuum models. Our simulations also predict a polarity sorting and periodic pattern formation in mixed polarity bundles on the slow time scales.

2. Model

We use computer simulations to calculate the dynamics and self-organization of the one-dimensional filament bundles cross-linked by the molecular motors. Actin and microtubule filaments are treated in a similar manner, as providing linear tracks for the motors. Our approach is intermediate between detailed molecular-level simulations that explicitly account for all the motors and filaments in the system[26] and continuum approaches that extend the diffusion-advection equations to include the motor-driven, active fluxes of the filaments.[22–25] The latter provide equations for the evolution of the filament densities; they successfully capture phenomena unique for active systems, such as filament sorting, bundle contraction and aster formation. The continuum approach, however, usually assumes pairwise interactions between the filaments, does not account for the dynamics induced in large, inter-connected filament clusters of filaments, and is therefore limited to the dilute motor densities. Our coarse-grained approach keeps track of every filament, but treats the motors in an averaged way, and allows exploring the filament dynamics both in loosely and in densely connected bundles.

A Bundle structure

We consider a cylindrical bundle consisting of N polar filaments, where $\alpha_L = N_L/N$ and $\alpha_R = 1 - \alpha_L = N_R/N$ are the fractions of the filaments oriented to the left and right, respectively. All filaments are of the same length L; the entire bundle's length (that is constant in some simulations and can change in the others) is L_B (Fig. 1). We assume that the filaments are closely packed in a hexagonal array where the cross-sectional distance between neighboring filaments is comparable to the size of a cross-linking molecular motor (~ 50 nm). For sufficiently high concentration of the motors, all M overlaps between neighboring filaments will be cross-linked by the motors. For smaller motor concentrations, both the fraction of the cross-linked overlaps, $\chi_b = M_b/M$, as well as the density of motors (per unit length) bound to the filaments, λ, will be lower. The parameter χ_b dictates the connectivity of the filaments in the bundle. For small values of χ_b, only pairs of filaments would interact, while for higher values, larger filament clusters including triplets, quadruplets, etc., would form. Above a characteristic threshold, χ_b^c, the bundle becomes mechanically percolated, i.e. interconnected from one side of the bundle to the other. The threshold value, χ_b^c, is a geometric property of the bundle that depends on the length of the filaments and their density (see below).

In order to show how the filament connectivity in the bundle influences its dynamic properties, χ_b and λ are treated as constant model parameters. These parameters are monotonically increasing functions of the motor concentration. Derivation of an exact formula for the dependence of χ_b and λ on the motor concentration requires additional assumptions and approximations about the nature of the filament-motor interactions; these are beyond the scope of the present paper. In addition, for the most part of this paper, we will be concerned with the bundles that are not subjected to external loads. In this case, simulations indicate that the length density of the motors, λ, plays a minor role, while connectivity parameter χ_b has a marked effect on the dynamics.

Since the bundle is one-dimensional, the most significant motion of the filaments is parallel to the principle axis of the bundle, which we denote as the x-axis. We thus ignore

stochastic, passive or active, lateral motion of the filaments in the $y - z$ plane. In the initial bundle configuration, we randomly place the filaments at various points along the x-axis and in the $y - z$ plane, so that no filaments 'collide' on the same line normal to the $y - z$ plane. During the subsequent one-dimensional motion of the filaments, however, it may happen that two filaments collide. Since the exact location of the filaments in the $y - z$ plane does not influence the averaged dynamics of the filaments, while the connectivity between the filaments does, we assume that when two filaments move past each other on the same line, they can maintain their interaction with the motors. This simplifying assumption avoids overly time-consuming calculations and has no effect on the results.

B Sliding of small filament clusters

We have investigated three types of cross-bridges that can form in the bundles of cytoskeletal filaments. Two of these types correspond to *unipolar* motors having motor domain at one end and binding domain at another, like dynein and kinesin-1, and to *bipolar* motors having motor domains at both ends, like kinesin-5 and myosin-2, as illustrated in Fig. 2. Usually the overlap region between neighboring filaments is large enough to accommodate several motors, so there could be more than one arrangement of the unipolar motors between the filaments. In one limit, the orientation of all motors is correlated, *i.e.* all motors have their motor domains on the same filament (Fig. 2a,b); we call this case *unipolar*. In the opposite limit, the motors bind the filaments independently of each other and their orientation is random; each filament will have an equal proportion of motor and binding domains attached to it, as illustrated in Fig. 2c,d; we call this case *bipolar*. The movement exerted by these two cross-linking configurations are similar for antiparallel filaments but different for parallel ones. Oppositely oriented motors in a cross-link between the parallel filaments exert forces in opposite directions inhibiting the filament gliding. Between the antiparallel filaments, the effects of the motors add up no matter what the orientation of the motors is. Bipolar motors such as myosin-2 or kinesin-5 that have the motor domains on

Fig. 2 Schematic illustration of three possible arrangements of molecular motors in interactions between neighboring filaments. Upper and bottom rows show parallel and antiparallel pairs of filaments respectively. Arrows show the direction of filament motion induced by the motors.

both sides also form the *bipolar* cross-links. The behavior in this case is similar to that of the uncorrelated unipolar motors as long as the two motor domains of the same motor exert their forces in an independent manner. While a bipolar cross-link consisting of the unipolar motors and one consisting of the bipolar motors may show a common averaged force-velocity relation as we illustrate below, they differ in at least one other respect: bipolar, but not unipolar, motors translocate between the parallel filaments. This, like other kinetic factors such as the on- and off-rates of the association of motors with the filaments, influences the life time of the cross-linking connection between two filaments. Such effects are not directly relevant to the present work and are included implicitly in the values of model parameters χ_b and λ.

C Model equations

Here we derive the equations used to calculate the filament movements. We assume that each bundle is cross-linked by only one motor type and that the motors at the filament overlaps are either completely correlated or randomly oriented as shown in Fig. 2. For each such overlap, we use a motor force-velocity relation to calculate the filament velocities. In the low Reynolds number environment of the cell,[27] the velocity, $\vec{v}_i$, of the ith filament is proportional to the total force, $\vec{f}_i$, applied to it by all motors connected to this filament:

$$\xi \vec{v}_i = \vec{f}_i, \qquad (2.1)$$

where ξ is the drag coefficient of the filament in the bundle. Typically, ξ is higher than the drag coefficient in aqueous solution due to a *weak* binding motor-filament interactions in the bundle that give rise to the so-called protein friction.[28] The drag coefficient value we used, 0.023 pN $\times$ sec/μm for 1 μm-long filament, is based on the diffusion constant measurements in ref. 28. In the simulations, this value was scaled by the filament lengths. For the bundles, since the motion is one-dimensional we define $\vec{f}_i = f_i \times \hat{x}$ and $\vec{v}_i = v_i \times \hat{x}$.

We assume that the motors stochastically associate with and dissociate from the filaments frequently, that the motors occupy the overlapping regions between neighboring filaments with the uniform density, λ, and that the force that the motors exert is additive and proportional to the total length l_{ij} of the overlap between the neighboring filaments. The mean motor number at the overlap is thus $\lambda \times l_{ij}$. Measurements of the force-velocity relations for some motors[29,30] suggest that the simplest—linear—relation is a reasonable approximation describing the motor mechanics. For simplicity, we also assume that the filament-associated motors share the load equally[31,32] and omit the complex nonlinear effect of indirect inter-motor interactions. Usually, the drag force resisting the movement of the 10 μm-long filament, $\xi v_i \sim 0.2$ pN $\times$ sec/μm $\times$ 0.2 μm/sec ~ 0.04 pN is much smaller than the characteristic stall force (in the pN range) of just one motor. Normally, more than one motor slides each filament,[11] so in the relevant limit, the effective viscous drag is negligible, and the total motor forces applied to each filament approximately balance to zero.

To use appropriate force-velocity relations, we have to distinguish between the different types of cross-links (Fig. 2).
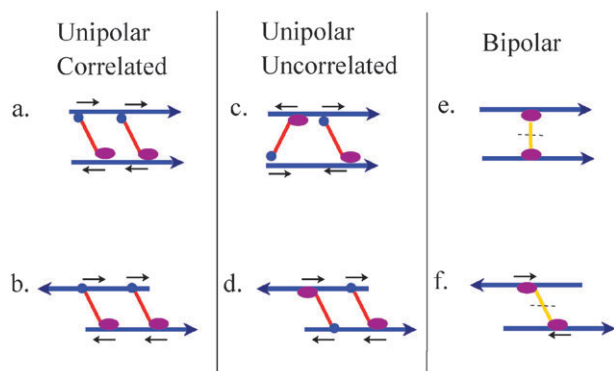
This journal is © the Owner Societies 2009

Phys. Chem. Chem. Phys., 2009, **11**, 4821–4833 | 4823

For the unipolar motors, the binding ('head') domain of the motor will be denoted by h, and the motor ('leg') domain—by l. For any particular motor (*e.g.*, kinesin/dynein), the 'leg' always moves toward the same (plus or minus) end of the filament, which in turn defines the orientation of the filament. Thus, the walking direction of the motor is the direction of the filament along the x-axis, $\hat{n}_i = n_i\hat{x} = \pm\hat{x}$. For instance, if $n_i = -1$ and the motor is minus-end directed, it means that the minus-end of that filament points in the negative direction of the x-axis.

(i) *Orientationally correlated unipolar motors*: we first consider the case when all motors within each overlap region are oriented in the same manner, *i.e.* they have their motor domains on one filament and binding domains on the other. Theoretically, this situation is expected when the binding of the motors to the filaments is highly coordinated and cooperative, for instance due to steric interactions between the motors or between the motors and the filaments. While not much is known about the orientation of motors in the crowded environment of these bundles, some indirect evidence for such an arrangement of motors exists, see refs. 33–36. Interestingly, we show below that the lower symmetry of this type of interaction gives rise to richer dynamics. For the correlated unipolar motors, we have the following force-velocity relation:

$$f_i = -\lambda l_{ij_h} f_s \left[n_i - \frac{v_{j_h} - v_i}{v_0} \right] = -f_{j_h}. \qquad (2.2)$$

In this notation, the subscript j_h means that the binding domains are associated with a neighboring filament j while the motor domains are connected to the filament i; the factors f_s and v_0 are the stall force and free velocity of the motors. The factor λl_{ij_h} in this formula is responsible for the additive forces of all motors at the overlap, and the expression in the square brackets describes the effective force decrease due to the relative filaments' sliding in the direction 'preferred' by the motors. For an interconnected bundle with multiple cross-linked regions of this form we have:

$$f_i = -\lambda f_s \sum_{j_h} l_{ij_h} \left[n_i - \frac{v_{j_h} - v_i}{v_0} \right] + \lambda f_s \sum_{j_l} l_{ij_l} \left[n_{j_l} - \frac{v_i - v_{j_l}}{v_0} \right], \qquad (2.3)$$

where the first sum corresponds to neighboring filaments that interact with the motors the binding domains of which are on the ith filament, while the second sum corresponds to neighboring filaments moved by the motors that interact with the motors the motor domains of which are on the ith filament.

(ii) *Orientationally uncorrelated motors*: when the association of the motor proteins to a pair of neighboring filaments is independent and orientationally uncorrelated, we sum the contributions of the two populations of motors in that overlap region; this leads to the following force-velocity relation:

$$f_i = \frac{1}{2} \lambda l_{ij} f_s \left[(n_j - n_i) + \frac{2(v_j - v_i)}{v_0} \right]. \qquad (2.4)$$

The factor 1/2 reflects the probability of a motor to associate with either of its ends with each filament. Note that for a parallel filament pair ($n_j = n_i$), eqn (2.4) predicts that if the

filaments do not move relative to each other ($v_i = v_j$), then the motor forces cancel each other, $f_i = 0$. In contrast, in the correlated motor case, the motors exert significant sliding forces on a pair of parallel filaments gliding with the same velocity. For an antiparallel pair, eqns (2.4) and (2.2) are equivalent. Thus, for antiparallel filaments there is no difference between the orientationally correlated and uncorrelated binding cases. Finally, to generalize eqn (2.4) for a bundle that consists of many cross-linked regions of orientationally uncorrelated motors, we write:

$$f_i = \frac{1}{2} \lambda f_s \sum_j l_{ij} \left[(n_j - n_i) + \frac{2(v_j - v_i)}{v_0} \right]. \qquad (2.5)$$

(iii) *Bipolar motors*: the bipolar motors' force-velocity relations are very similar to those of the uncorrelated unipolar motors assuming that the motors generate forces independently of each other. If such motor is connected to a pair of filaments, i and j, it exerts equal and opposite forces $f_i = -f_j$ on them. Using the linear force velocity relation for each of the motor domains, we have: $f_i = -f_s[n_i - (v_m - v_i)/v_0]$ and $f_j = -f_s[n_j - (v_m - v_j)/v_0]$. We thus find the equation for the velocity of the motor between two filaments sliding with velocities v_i and v_j: $v_m = \frac{1}{2}[v_i + v_j + v_0(n_i + n_j)]$. Substituting this formula into the expression for f_i, we find:

$$f_i = \frac{1}{2} f_s \left[(n_j - n_i) + \frac{v_j - v_i}{v_0} \right]. \qquad (2.6)$$

Thus, for a bundle that is cross-linked by the bipolar motors, we have:

$$f_i = \frac{1}{2} \lambda f_s \sum_j l_{ij} \left[(n_j - n_i) + \frac{v_j - v_i}{v_0} \right]. \qquad (2.7)$$

The only apparent difference between the bipolar and uncorrelated unipolar motors is that bipolar motors slide the antiparallel filaments with free velocity that is twice as large as that generated by the uncorrelated unipolar motors. For this reason, below we discuss only two cases: the correlated unipolar motors, which we simply call from now on unipolar motors, and the bipolar motors. The results for the bipolar and uncorrelated unipolar motors are qualitatively similar.

Some previous models assumed that the motors 'linger' at the filaments' ends.[22,24,25] As a result, the motors with such properties have a tendency to focus the similar filament ends together.[22] Effectively, this leads to emergence of loose and dynamic 'sarcomeres' in which two or more filaments have, for example, plus ends in the middle of the cluster and minus ends sticking out. The bipolar motors then tend to converge many clusters like that, similarly to bipolar myosin-2 contracting the actin sarcomeres in muscle and stress fibers. In contrast, in this paper we implicitly assume that the motors 'slide off' the filament ends without delay upon reaching the ends. As a result, the individual filaments in our model tend to slide past each other, and our simulations never produce the contractile behavior characteristic for some actin-myosin systems that was captured by some of the earlier models.[22]

Eqn (2.1) together with eqns (2.3), (2.5) or (2.7) (for each of the filaments in the bundle) constitute the self-consistent set of algebraic linear equations for the forces and velocities of the

filaments. The computational procedure underlying the simulations is as follows: at each computational step, the inter-filament overlaps are identified for the given bundle's spatial configuration, and the fraction of the overlaps determined by the parameter χ_b is randomly assigned to be associated with the motors. Then, a linear solver determines the velocities of each filament, and the filaments are propagated along the x-axis by a small distance, $v_i \times dt$, where $dt \sim 0.1$ sec is the time step sufficiently small compared to the characteristic time of the interactions between the neighboring filaments. We generated the initial filament positions using a random uniform distribution and simulated the bundle dynamics for each of these initial distributions for a time sufficient to detect essential bundle's behavior. Repeated, this procedure results in trajectories of the filaments in the bundle that can be averaged (over the ensemble of initial bundle configurations and/or time, as described below) providing quantitative description of the bundle's behavior.

D Typical interactions in small clusters of parallel filaments

The filament dynamics in large interconnected bundles is very complex, which is exactly the reason for explicit computer simulations, so to build intuition for the analysis of the dense bundles, it is useful to consider small filament-motor clusters first. Fig. 3 illustrates clusters of three and five parallel filaments bundled in a cylindrical fashion connected by the unipolar motors in a number of different ways. In the appendix, we provide the analytical solutions of the algebraic eqns (2.1), (2.3) for all these cases.

The most interesting filament-motor clusters in Fig. 3a,d show an interaction type that we call 'telescopic'. This special configuration is defined by three requirements: (1) the whole bundle is interconnected (there are no two sub-bundles not connected by the motors to each other), (2) in any sub-cluster of three filaments, there are only two interconnected overlaps, and (3) for any filament that is connected to two other filaments, motors in one of these connections are associated with the given filament with the binding domain, and in another connection—with the motor domain. These filament clusters 'open' like 'telescopes': the filament in the middle stays put, two filaments next to it slide to the right and left with the speed almost equal to the free motor gliding rate, next two filaments slide in the 'piggy-backing' fashion on those two filaments with similar relative rate, and so on. The calculations in appendix show that in the absence of the external load and when the drag on the filaments from the protein friction is negligible, the filaments at the end of the 3-filament telescopic cluster (Fig. 3a) slide outward with the free motor speed v_0, while the filaments at the end of the 5-filament telescopic cluster (Fig. 3d)—with the speed $2v_0$. It is easy to demonstrate that in this limiting case (no load and low drag), the velocity of the filaments in the telescopic cluster of N filaments is sequentially augmented and linearly graded toward the cluster edges, so that the filaments at the ends of the bundle spread out with the speed $\frac{1}{2}(N-1)v_0$, several times greater than the free motor speed.

In the interconnected telescopic clusters, the minimal possible number of inter-filament overlaps are occupied by the motors. If additional motors are added, so that all three pairs in the sub-clusters of three filaments are connected by the motors (Fig. 3b–c,e–h), then the filaments' gliding slows down. For example, if the third motor is added to the 3-filament cluster, this third motor acts as either 'soft' (Fig. 3c) or 'hard' (Fig. 3b) brake: in these cases, the speed of the filaments at the ends slows down from v_0 to $2v_0/3$ and to zero, respectively. Similarly, just one additional motor slows down the speed of the edge filaments in the 5-filament cluster from $2v_0$ to $5v_0/3$ (Fig. 3h), $4v_0/3$ (Fig. 3f), v_0 (Fig. 3g) and $2v_0/5$ (Fig. 3e).
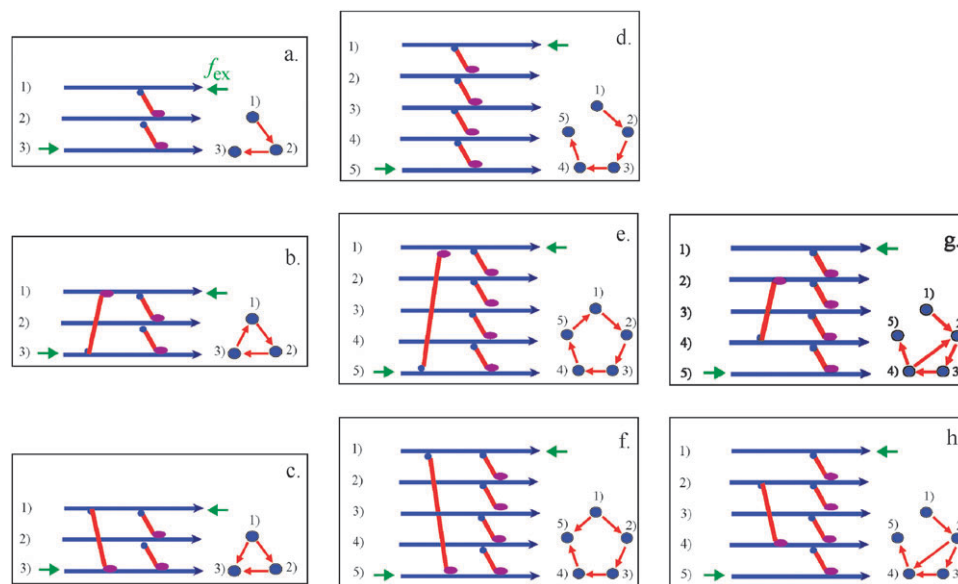

Fig. 3 Several examples of small clusters of 3 and 5 parallel filaments. The figure shows the connectivity between the filaments; right diagrams show a cross-sectional view of the cluster (with arrows denoting the motor domains). Panels a and d show ideal 'telescopic' configurations; other panels show more crowded connections that lead to slower dynamics of the filaments. See the text for details and the appendix for analytical solutions of the equations of motion for these clusters.

This journal is © the Owner Societies 2009

Phys. Chem. Chem. Phys., 2009, **11**, 4821–4833 | 4825

Comparing the 5- and 3-cluster cases suggests that dense long filament bundles would still exhibit the telescopic property only partially diminished by some motors acting as 'brakes': the more filaments there are in the bundle, the more 'piggy-backing' effect will lead to the acceleration of the filaments at the bundle edges. In the following sections, we show how these considerations are manifested in the dynamics of the large bundles subject to various boundary conditions. We emphasize that this telescopic effect is the property of the unipolar motors; the bipolar motors simply try to equalize speeds of the parallel filaments.

3. Results of computer simulations

We simulated hundreds of bundled filaments of equal length $L = 10$ μm that were initially randomly and uniformly distributed over the distance of tens to hundreds of microns in a tightly packed bundle configuration. In all simulations, the total stall force of the characteristic number of motors per filament was at least an order of magnitude greater than the effective viscous drag force per filament. In the computer experiments, we varied (1) initial filament density, (2) boundary conditions, (3) bundle motor-mediated connectivity, (4) polarity (fraction of left- and right-oriented filaments),

(5) type of motors (unipolar and bipolar). In this section, we describe the resulting bundle dynamics in all these different cases.

A Free expansion and sorting of filament bundles

Several characteristic properties of the dynamics and self-organization of the one-dimensional bundles can be demonstrated on the simple example of a free expansion of a mixed-polarity bundle: An equal mixture ($N_L = N_R = 50$) of right- and left-oriented filaments of equal length $L = 10$ μm, initially arranged in a short ($L_B = 20$ μm) homogeneously mixed bundle, was allowed to expand freely. In this simulation, the bundle is saturated with motors so that all filament overlaps are cross-linked by motors ($\chi_b = 1$). The dynamics of such bundles cross-linked by either unipolar or bipolar motors are shown in Fig. 4.

The bipolar motors 'sort out' the bundle in a very simple way: filaments of the same polarity do not move relative to each other, while two sub-populations of the opposite polarity filaments slide past each other with the constant speed that is twice the free velocity of the motor domains, $2v_0$ (Fig. 4a–c). Fig. 4b shows that the density profile of each filament sub-population maintains its uniform shape and drifts at the
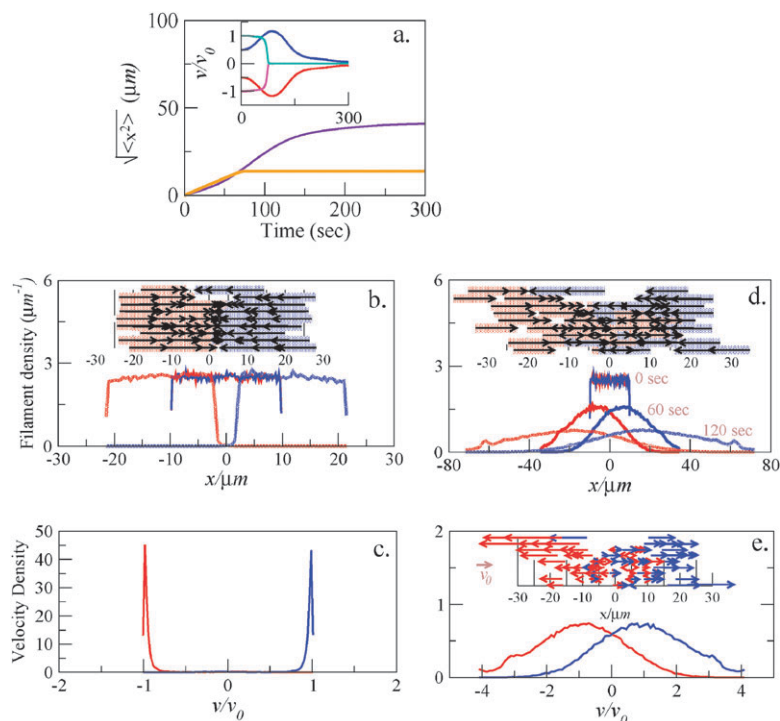

Fig. 4 Free expansion and spontaneous sorting of the mixed polarity bundles. Besides the 'snapshots' of the filament spatial distributions and velocity fields across the bundle, we also show the plots of: (1) average filament displacement as a function of time defined as $\sqrt{\langle x(t)^2 \rangle} = (\sum_{i=1}^{N}(x_i(t) - x_i(0))^2/N)^{1/2}$, where $x_i(t)$ is the position of the center of the ith filament at time t; (2) average filament velocity as a function of time defined as $\langle v(t) \rangle = \sum_{i=1}^{N} v_i(t)/N$, where $v_i(t)$ is the velocity of the ith filament at time t; (3) filament density at given times defined as the number of filaments that have any of their parts in a segment of unit length at given location; (4) velocity density at given times defined as the number of filaments that have their velocities in the unit velocity interval. a. The average filament displacement $\sqrt{\langle x^2 \rangle}$ as a function of time for the two motor types (unipolar in purple, bipolar in orange). The inset shows the average velocity of the left- (blue/cyan) and right- (red/pink) oriented filaments; lighter colors are for bipolar motors. Panels b (bipolar) and d (unipolar) show the respective filament density plots at several times; the insets shows simulation snapshots of the bundle at $t = 60$ sec. Panels c (bipolar) and e (unipolar) compare the velocity distributions at $t = 60$ sec. The inset in panel c shows the velocity field at $t = 60$ sec. Blue/red arrows are for the left/right-oriented filaments; the arrow shows the direction of movement and its length is proportional to the speed of the filament. All curves are for the high motor density case ($\chi_b = 1$).

constant speed (see the narrow velocity distribution of the filaments in Fig. 4c). The average filament displacements thus increase linearly with time for $t \sim 70$ sec until the sliding stops abruptly when the bundle is entirely sorted out into two sub-bundles of parallel filaments with no overlap between them (Fig. 4a).

The interaction between the filaments moved by the correlated unipolar motors results in richer dynamics. In this case, too, the mixed bundle is unstable and is sorted out into two sub-bundles of parallel filaments (Fig. 4a,d–e). The relative sliding velocity of the sub-bundles, however, is not constant: the filaments accelerate up to $t \sim 70$ sec and then decelerate at later times. This observed acceleration of the filaments at early times is the result of the telescopic expansion of the bundle, in which the filaments are moving faster near the edges (Fig. 4e). In the beginning, when the bundle is dense, too many motor-mediated connections between the parallel filaments work as 'brakes', then partial expansion lowers the density and makes the number of inter-filament connections optimal for the telescopic expansion. Yet later, the bundle density decreases so much that the filaments gradually loose their contacts with other filaments in the bundle, sliding becomes infrequent, and the spread slows down. The motion at later times becomes diffusive (Fig. 4d). The filaments in the parallel sub-bundles, besides drifting away from the bundle center, are performing a random walk in one dimension being actively pushed bidirectionally by the motors, so that the filament velocity distribution is Gaussian (Fig. 4e).

B Effects of motors density and boundary conditions on filament dynamics

The previous simple example shows that the filament dynamics depends not only on the type of the motors and bundle polarity, but also on the internal structure and connectivity in the bundle. To understand these dependencies in detail, we investigate the differences between loosely and densely connected bundles. We start with the bundles of parallel filaments, and because bipolar motors have no effect on the parallel filaments, we only consider the case of the unipolar motors. To investigate the dependence of the dynamics on the filament density, we simulated (1) ringed bundles of the constant lengths with periodic boundary conditions, and (2) 'free open' bundles of the constant lengths with absorbing boundary conditions, so that the filaments crossing the bundle ends disappear, while new filaments are constantly nucleated at random positions in the bundle at a rate that guarantees a constant total number of filaments (Fig. 5c).

Fig. 5 shows the filament trajectories and velocities in these bundles for various fractions of active (motor-linked) overlaps and filament densities. As expected, there are no boundary effects when the motor density is low ($\chi_b \lesssim 0.1$) and only small clusters of filaments form in the bundle. At these concentrations, the filaments perform a random walk with long pauses (Fig. 5b) that result from long periods of no contact with any motors. These long pauses result in the sub-diffusive behavior of the filaments (data not shown). The average
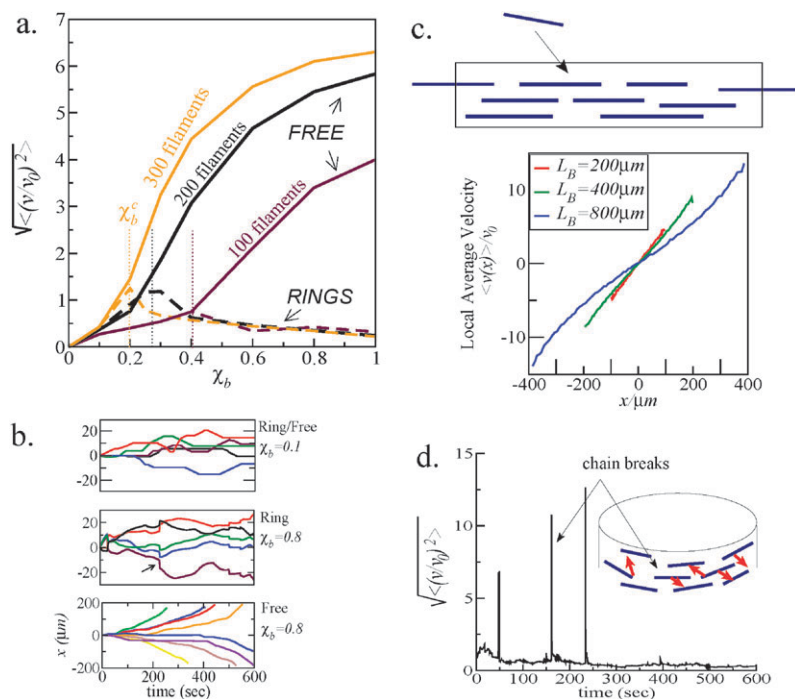

Fig. 5 Comparing the filament dynamics in free and open *parallel* bundles with that in ringed parallel bundles. (a) The average filament speed as a function of the active cross-bridge fraction, χ_b, for three values of density (100, 200 and 300 filaments per 400 μm-long bundle), and for two different boundary conditions. (b) Several typical filament trajectories in the 200-filament bundle for various connectivities and boundary conditions. (c) Average spatial velocity profiles in free bundles of three different lengths showing the graded filament velocity. (d) Occasional breaking of closed chains of filaments in dense ringed bundles ($\chi_b = 0.8$) causing rapid spikes of sliding. The average velocity was calculated as in Fig. 4. The average spatial velocity profiles were computed by recording the velocities of the filaments passing through given locations and averaging these velocities over long time intervals.

filament velocities increase linearly with the connectivity parameter χ_b and are smaller than the free motor velocities (Fig. 5a).

At higher motor and/or filament densities, we find a qualitatively different dynamics once a threshold fraction of active cross-bridges is reached. This threshold fraction corresponds to a percolation transition in which interconnected clusters of filaments spanning the entire length of the bundle form. This percolation threshold is a geometric property of the three-dimensional hexagonal organization of the filaments in the $y - z$ plane and their spread along the x-axis. The numerical value of the threshold fraction depends on both the length density of the filaments, N/L_B, and on the filament length. We find that χ_b^c varies from ~ 0.2 for 300 filaments to ~ 0.4 for 100 filaments. For comparison, the bond-percolation threshold is 0.34 for a two-dimensional triangular lattice and 0.25 for a three-dimensional cubic lattice.[37]

When $\chi_b > \chi_b^c$, the behaviors of the open and closed (ringed) dense bundles are drastically different. In the free bundle with open edges, the filaments expand rapidly, with speeds a few-fold greater than the free motor speeds (Fig. 5a). The average filament speed increases as a function of both the filament and motor density (Fig. 5a), however, this increase is smaller when the densities become too high (Fig. 5a) because too many motors work as brakes in very dense bundles. Fig. 5b,c shows that the speed of individual filaments increases toward the bundle ends, that the speed is graded approximately linearly across the bundle, and that the maximal velocity at the bundle ends increases with the bundle length. These effects result from the telescopic interactions that develop in the highly connected bundles. Small nonlinearities of the velocity profiles seen most prominently in the long bundles (Fig. 5c) stem from the lower filament density near the edges.

In the ringed morphology, the filaments form closed circular chains at $\chi_b > \chi_b^c$. The filaments movements becomes significantly slower than those in the open bundles (Fig. 5a,b). Above the percolation threshold, the average filament speed does not depend on the filament density and decreases with χ_b (when more connections 'lock' the filament chains together). Fig. 5d shows an interesting behavior of the dense ringed bundles of parallel filaments: once in a while, the closed interconnected filament chains get disconnected at random positions and open up. These transient events (appearing as speed spikes in Fig. 5d and as jumps of the individual filament trajectories shown with the arrow in Fig. 5c) lead to very brief episodes of rapid filaments' gliding. While these events are aperiodic and infrequent, they are typical for the dense parallel ringed bundle.

Fig. 6 summarizes the dynamics of the mixed bundles with unipolar motors in open and ringed geometries for high and low motor densities. After a short equilibration period (~ 200 sec), the filament velocity distribution reaches a quasi-steady state. (We show below that for low-density bundles, the velocity decrease after ~ 100 min due to a peculiar pattern formation.) As expected, for low values of χ_b, the motion of the filaments is independent of the boundary conditions: the velocity distributions are essentially the same
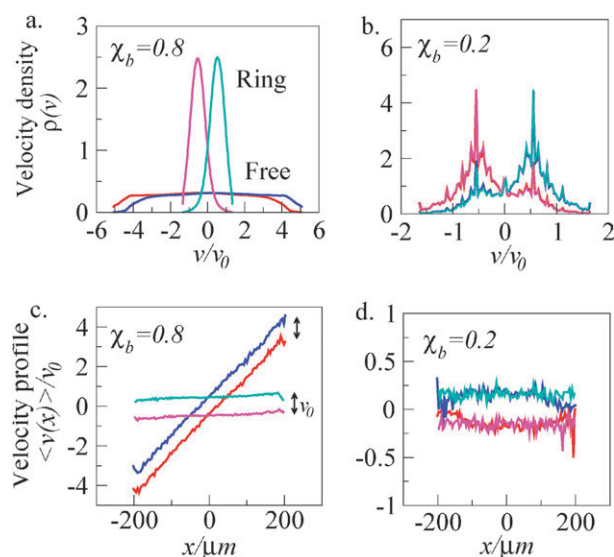

Fig. 6 Dynamics in ringed and open *mixed* polarity bundles of length $L_B = 400$ μm with $N_R = N_L = 200$ filaments cross-linked by the correlated unipolar motors. Upper panels show velocity distributions for all filaments averaged over time and space; lower panels show time-averaged velocity profiles along the x-axis computed as described in Fig. 5. Blue/cyan colors are for left-oriented filaments; red/pink colors are for right-oriented filaments; the lighter colors are for the ringed bundles. The calculation of the velocity distributions included only filaments that have at least one motor-mediated connection to other filaments and excluded all those filaments that are unconnected and thus stationary in the bundle. At low cross-bridge densities (right panels), there is no difference between the two bundle geometries. Right oriented filaments (red/pink) move mainly to the left and left oriented filaments (blue/cyan) move mainly to the right. For densely interconnected bundles (left panels), there is a profound influence of the boundary condition on the filament dynamics. The ring morphology of the bundle results in significantly slower motion of the filaments. In contrast, in the free bundle the velocity distribution is wide and flat (a) and the velocity profile is graded along the bundle axis. Interaction between *antiparallel* filaments leads to an average difference of v_0 between the two sub-populations of filaments. In addition, in the open bundle, the filaments expand in spatially graded telescopic fashion.

in the open and ringed bundle (Fig. 6b,d). The filament velocities are independent of the location. The variance of the velocities is high, but most of the left/right-oriented filaments glide to the right/left.

In contrast, at high motor densities, the behavior is drastically different in the ringed and open bundles (Fig. 6a,c). In the open bundles, the velocity distributions of the filaments are wide and flat, while in the ringed bundle, they are peaked around $\pm v_0/2$. In the dense open bundles, filaments of the same orientation organize into two telescopic sub-bundle expanding in the linearly graded way (Fig. 6c), so that the filament velocities are proportional to the distance from the center of the bundle. In contrast, in the ringed bundle, these two sub-populations are locked together. In addition, in both geometries, two sub-bundles glide relative to each other with the free motor velocity.

Dynamics of the mixed bundles cross-linked by the bipolar motors is shown in Fig. 7. Unlike for the unipolar motor
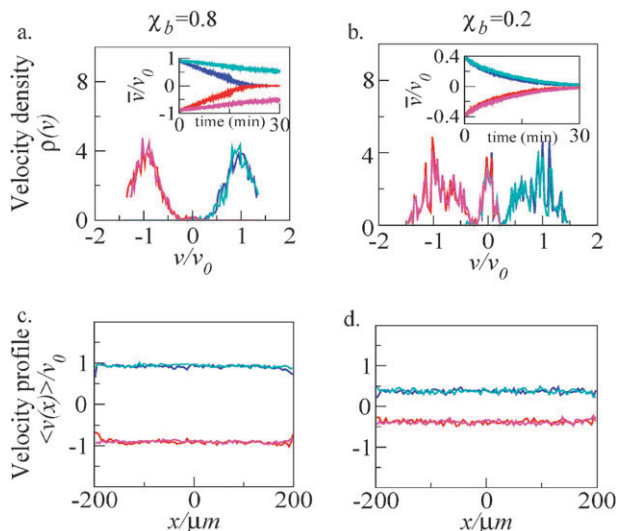
Fig. 7 Dynamics in the mixed bundles powered by the *bipolar* motors. All parameters and averaging are the same as in Fig. 6. Upper panels show averaged velocity distributions and lower panels show velocity profiles along the *x*-axis 2 min after the simulation started. Blue/cyan colors are for left-oriented filaments and red/pink colors for right-oriented filaments; the lighter colors are for the ringed bundles. The insets in panels a,b show slow decrease of the filament movements due to formation of the polarized domains.

bundles, no telescopic interactions develop because parallel filaments do not move relative to each other, so there is no significant effect of either geometry or motor density on the filament movements. The only 'trivial' effect is that at lower motor densities, a greater fraction of filaments is unconnected to other filaments and so the average velocity of the filaments decreases. On the average, left/right-oriented filaments glide to the right/left; there is no dependence of the velocities on the location in the bundle. Interestingly, the insets in Fig. 7a,b show that the mean velocities slow down with time on the scale of tens of minutes. This effect is a consequence of the filament sorting and formation of parallel clusters of filaments (discussed in detail below) that can no longer be moved by the bipolar motors.

C Effective diffusion and drift in loosely connected bundles

In the loosely connected bundles, where the fraction of active overlaps between the filaments is smaller than the percolation threshold, $\chi_b < \chi_b^c$, only small interconnected filament clusters form transiently, and the dynamics is independent of the bundle geometry. In this case, we observed that the individual filaments undergo effective drift and diffusion (Fig. 8). We focus here on the bundles with the unipolar motors where the dynamics is more interesting and use periodic boundary conditions to ensure a constant average filament density.
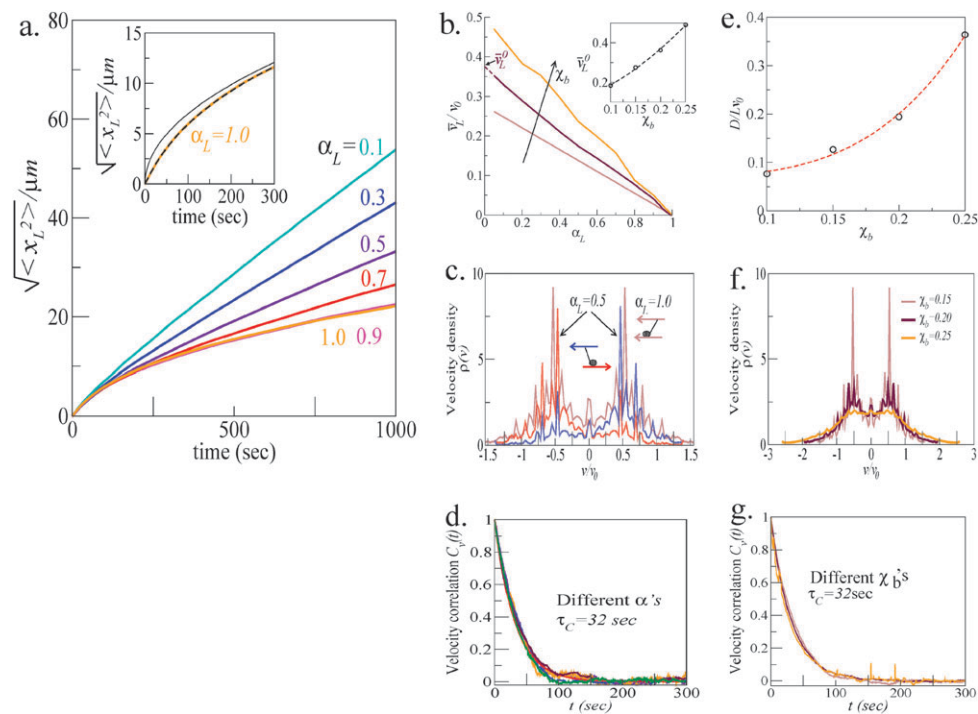

Fig. 8 Diffusion-drift dynamics of loosely connected bundles with the unipolar cross-bridges. (a) The average filament displacement as a function of time for various mixtures of right and left oriented filaments. The inset shows this function for a parallel bundle in the first 300 seconds; dashed line is a fit to eqn (3.8), solid line is the fit to the Einstein relation, $\langle x_L^2 \rangle = 2Dt$. (b) The drift coefficient as a function of the polarity ratio for various values of the parameter χ_b. The drift increases with χ_b as seen in the inset. (c) Typical velocity distributions of the right- (blue) and left-(red) oriented filaments in the mixed bundle ($\alpha_L = \alpha_R = 0.5$) and of all filaments in the parallel bundle for $\chi_b = 0.15$. In the parallel bundle, the filaments move bidirectionally and the distribution is symmetric. In the mixed bundle, right/left-oriented filaments move mainly to the left/right. (d) The velocity correlation function $C_v(t) = \langle (v_L(t) - \bar{v}_L)(v_L(0) - \bar{v}_L) \rangle / \langle (v_L(0) - \bar{v}_L)^2 \rangle$ as a function of time for various values of the polarity ratio and for $\chi_b = 0.15$. (e) Effective diffusion coefficient as a function of χ_b. (f) Typical velocity distributions in the parallel bundles for various values of χ_b. (g) The velocity correlation function in the parallel bundle as a function of time for various values of χ_b.

This journal is © the Owner Societies 2009

Phys. Chem. Chem. Phys., 2009, **11**, 4821–4833 | 4829

Fig. 8a shows the average filament displacement as a function of time for four cases of the bundle polarity: $\{\alpha_L, \alpha_R\} = \{0.0, 1.0\}, \{0.1, 0.9\}, \{0.3, 0.7\}, \{0.5, 0.5\}$. For all these cases, we found that the following expression:

$$\langle x_L^2 \rangle = 2Dt\left[1 - \frac{\tau_C}{t}\left(1 - e^{-t/\tau_C}\right)\right] + \bar{v}_L^2 t^2 \qquad (3.8)$$

fits very well the average left-oriented filament displacement obtained from the numerical simulations (Fig. 8a) indicating that effectively the filaments undergo the superposition of drift with the constant rate $\bar{v}_L$ and diffusion characterized by the constant diffusion coefficient D. An equivalent equation holds for the right-oriented filaments, with a different drift velocity. The average drift velocities of the right- and left-oriented filaments obey the following relation: $\alpha_L \bar{v}_L = \alpha_R \bar{v}_R$, so there is no average filament flux in the mixed-polarity bundle. Thus, in an uneven mixture of filaments, the filaments in minority effectively drift unidirectionally by interacting mainly with oppositely oriented filaments. In contrast, the filaments in majority mainly interact with alike filaments, and their motion is essentially diffusive. Fig. 8c shows the velocity distributions in the bundles.

Fig. 8b shows the mean filament speed as a function of the fraction of the filaments of this polarity in the bundle. We find the linear relation between the speed and polarity: $\bar{v}_L/v_0 = v_L^0(1 - \alpha_L)$, where v_L^0 is an increasing function of the fraction of active overlaps in the bundle, χ_b. This numerically established linear relation supports assumptions made in the earlier models.[22]

In eqn (3.8), parameter τ_C is the sliding correlation time, which turns out to be approximately equal to 30 sec (Fig. 8d): for approximately 30 sec, the filaments persistently slide past each other until they engage with other filaments and change their velocity. The correlation time is independent of the polarity ratio α and of the parameter χ_b (Fig. 8d,g). We found in the simulations that $\tau_C \sim L/v_0$ (data not shown), so the correlation time increases with the filament length and decreases with the free motor velocity.

For times longer than τ_C, the filaments perform a one-dimensional random walk. We found that the filaments' effective diffusion coefficient, D, is of the order of $L \times v_0$, so it is an increasing function of the filament length and free motor velocity. The diffusion coefficient also increases with the bundle connectivity χ_b (Fig. 8e) due to the increase of the width of the velocity distribution in larger interconnected filament clusters at higher connectivity (Fig. 8f). The magnitude of the effective diffusion coefficient is $D \sim 0.1\ \mu m^2/sec$ for $L = 2\ \mu m$ and $v_0 = 0.2\ \mu m/sec$. This value is comparable to the thermal diffusivity of a 2 μm-long free microtubule in an aqueous solution;[28] of course, the stochastic motion of a filament in a bundle is not due to the thermal agitation, but results from the motor-generated sliding. Note that while the thermal diffusion decreases with the filament length, the effective motor-dependent diffusion increases with L.

The diffusion-drift dynamics of individual filaments predicted by the simulations are consistent with the Langevin model:[38]

$$\frac{dv}{dt} = -\frac{v}{\tau_C} + \frac{\bar{v}}{\tau_C} + f_r \qquad (3.9)$$

with the random force f_r. From the solution of the Langevin equation[38] one can derive eqn (3.8) and the exponential decay of the velocity correlation function.

D   Filament sorting and pattern formation in the bundle

As noted above, when we investigated the velocity distributions, we noticed that the quasi-steady state distributions evolved on the scale of minutes, but then very slow changes in the filament positions and velocities began to emerge on the scale of tens of minutes. To understand these processes, we simulated long filament bundles for a few hours (of real, not computational time). We used the periodic boundary conditions, but the open bundles behaved similarly (data not shown). The results exhibited in Fig. 9 demonstrate the unexpected phenomenon of the spontaneous pattern formation: on the scale of tens of minutes, periodically arranged unipolar domains of filaments started to emerge in the bundles where equal fractions of the right- and left-oriented filaments were initially uniformly mixed.

To trace the domain growth dynamics, we calculated the spatial polarity correlation function $C_n(d) = \langle n(d)n(0) \rangle$ where the average is taken at a given time over all filaments in the bundle and for all of hundreds of simulated bundles. Here d is the distance along the x-axis between each given filament and any other filament in the bundle; $n = \pm 1$ is the respective filament polarity. Typical plots of the polarity correlation function are shown at consecutive times as insets in Fig. 9. These plots demonstrate that for both loose and dense bundles with the bipolar motors and loose bundles with the unipolar motors, the polarity correlation is positive for small distances, negative for greater distances, and then the filaments get uncorrelated at yet greater distances. This behavior implies that, on average, any filament in the bundle is surrounded by similarly oriented filaments in its vicinity and by oppositely oriented filaments at longer distances. The first zero of the correlation function is the average size of the unipolar filament domain, or the pattern period.[39] The characteristic size of the unipolar domains is a few tens of microns (few filament lengths), and it grows with time in a sub-linear manner (Fig. 9). Tracing the evolution of this period with time allows us to calculate the growth rate of the unipolar domains (Fig. 9).

For the low unipolar motor density (Fig. 9a), this pattern formation can be explained qualitatively as follows: interactions between the antiparallel filaments give rise to the relatively fast local sorting of the filaments by their polarity, as in Fig. 4. Then, interactions between the parallel filaments in the unipolar domains result in a slower diffusive motion that gradually increases the domain size. Whenever a filament of the opposite polarity moves into such domain, this filament rapidly slides to the neighboring domain—this keeps the polarity separation. The plots of the correlation function $C_n(d)$ show that the domains grow sub-linearly with time, $\langle d \rangle \sim t^{0.65}$. Interestingly, a similar characteristic time dependence with a power law of $t^{2/3}$ is known in the process of spinodal decomposition in unstable liquids or solids in the inertial regime, where de-mixing happens spontaneously throughout the system.[39] In contrast, densely connected bundles ($\chi_b = 0.8$) with the unipolar motors remain

4830 | *Phys. Chem. Chem. Phys.*, 2009, **11**, 4821–4833

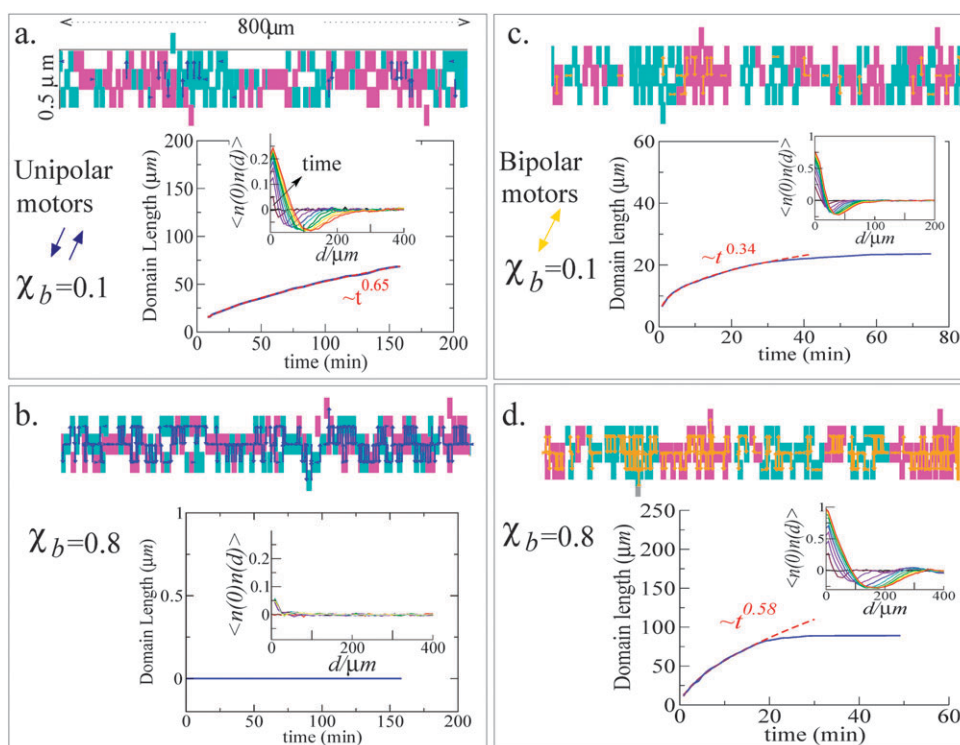This journal is © the Owner Societies 2009

Fig. 9 Polarity sorting and domain formation in the mixed polarity bundles. 800 μm-long bundles consisting of $N_L = N_R = 200$ filaments were simulated with periodic boundary conditions. The panels show the bundle configurations (a,b—unipolar, c,d—bipolar motors; a,c—loose, b,d—dense bundles) evolved in 1.5 hour from the initial random uniform filament distribution. The upper parts of the panels show the projections of all filaments onto the $x - z$ plane. Each bar represents a 10 μm-long filament (blue/pink code the left/right-oriented filaments, respectively). Small arrows represent the active cross-bridges (blue/yellow arrows stand for the unipolar/bipolar motors, respectively). The lower parts of the panels show the average lengths of the unipolar filament domains (pattern period calculated from the correlation function, see text) as functions of time. The insets plot the polarity correlation function as a function of the inter-filament separation d for every 200 sec (changing from cold to hot colors).

homogeneously mixed and *no* ordering is observed as seen in Fig. 4b. The explanation for this behavior relies on the formation of the long-range telescopic interactions. These interactions result in global correlations of the filaments across the whole bundle, which, as far as the filament polarity is concerned, mixes the bundle.

Similarly, the bundles with the bipolar cross-bridges (Fig. 4c,d) self-organize into the periodic patterns, alas at both small and high motor density, because in this case the telescopic interactions do not form as the bipolar motors do not exert forces on the parallel filaments. For the same reason, the bipolar motors do not generate the effective diffusion within the unipolar filament domains, so the domain size increases much slower with time in this case (as $\sim t^{1/3}$ for the loose bundles compared to $\sim t^{2/3}$ for the unipolar motors). The rate of the domain size increase grows with the bundle connectivity χ_b (Fig. 4c,d) because in the denser bundles more motors shuffle the filaments more vigorously.

4. Discussion

Our computational study predicts the rich variety of dynamics exhibited by the filament-motor bundles. First, when the bundles are 'loose' (less than 25–30% of the overlaps between the neighboring filaments are cross-linked by the motors), the filaments undergo effective diffusion and drift. We find that the

drift rate for a given filament is the linear function of the density of the opposite polarity filaments, which supports the assumption of the quasi-local continuous approach pioneered in ref. 22. The drift rate increases with the connectivity of the bundle. Our theory gives the estimate of the effective diffusion coefficient resulting from the active motor sliding, which is of the order of the motor speed multiplied by the filament length, and is not sensitive to the bundle density and polarity. This estimate gives a mechanistic support to the earlier phenomenological theories.

Second, our simulations demonstrate the nonlocal behavior of the dense bundles not captured by the earlier models. We predict that when more than 25–30% of the overlaps between the neighboring filaments are cross-linked by the motors, the percolation transition takes place, and the whole bundle becomes interconnected. In this case, drastically different behaviors are exhibited by the bundles with free ends and by the bundles closed into a ring, and in the cases of the uni- and bipolar motors. For the ringed bundles, any type of motors simply 'lock' the filaments in two sub-bundles of the left- and right-oriented filaments, and then these two sub-bundles slide relative to each other with the free motor speed. Same behavior occurs in the open bundles cross-linked by the bipolar motors. However, a novel phenomenon of the 'telescopic' expansion takes place in the open bundles cross-linked by the unipolar motors that bind in the same

orientation within each inter-filament overlap. In this case, each sub-bundle of the parallel filaments expands rapidly, and the filament velocities are increasing linearly in space from the center of the bundle outward. Due to the 'piggy-backing' effect,[15] the filaments near the edges of the bundle can slide with rates that are much greater than the speeds of the individual motors.

Finally, our simulations make important novel prediction about the self-organization and sorting phenomenon in the mixed-polarity bundles that takes place on the scale of the tens of minutes. The simulations suggest that a homogeneous mixture of the filaments of the opposite polarity is unstable, and that the bundle spontaneously sorts out to form periodic clusters of filaments of the opposite polarity, because any antiparallel filament is rapidly moved by the motors into the neighboring opposite cluster, while the parallel filaments within the cluster move relative to each other slowly. Nevertheless, even parallel filaments disperse; as a result, the period of the pattern, which is initially equal to a few filament lengths slowly, in a sub-linear way, increases.

This pattern vaguely resembles the periodic structure of the actin-myosin stress fibers, and there is a possibility that the predicted phenomenon is a part of a gamut of processes responsible for the stress fiber organization. We emphasize again that we did not test the possibility of the motors 'lingering' at the filament ends. Earlier models[22] established that in that case a contraction of the bundle (behavior not captured by our theory) is possible due to transient quasi-sarcomere structures in the bundles.

The existent experimental data is not detailed and quantitative enough for a detailed comparison of the simulations with the experimental results. Many types of, for example, microtubule bundles in cells are known, both consisting of parallel (in neurons[7] and kinetochore fibers[15]) and mixed-polarity (in dendrites[40] and in the proplatelet shafts[6]). In most cases, it is unclear how many types of motors cross-link the bundle, and what are the errors and artifacts of the velocity measurements. However, there are some early indications that soon the quantitative experiment/theory comparison will be possible. A narrow velocity distribution in the *ringed* bundles has been reported recently for the annular microtubule bundles in blood platelets,[41] as predicted by our theory. On the other hand, a wide velocity distribution in the *open* bundles of the mitotic spindle has been observed,[12] again in agreement with one of our predictions. Perhaps in the future some other detailed predictions, such as the estimates of the effective diffusion and drift rates and bursts of gliding in the ringed bundles, can be tested.

Before such tests take place, however, our model has to include a number of factors omitted in this study for simplicity. First, the cell biological bundles consist of the filaments of variable lengths, and there are indications of a qualitatively different behavior among long and short sub-populations.[7] Second, usually the filaments turn over relatively rapidly.[42] Third, the bundles are often subject to the external forces—for example, we did not consider the possibility that the ringed bundle expands or contracts (like in the cytokinetic ring), because to make such simulation meaningful, one has to consider the physical effects of

curvature, cell cortex tension, *etc*. Last, but not least, some of the motors are very likely to connect the bundles to other cytoskeletal structures in the cell, and usually more than one type of motors cross-link the filaments. Despite these limitations, our model is the step necessary for mechanistic understanding of the cytoskeletal dynamics.

Appendix

We provide here the closed-form expressions for the velocities of the filaments in the clusters of Fig. 3. In the equations below, all velocities marked with the tilde sign are scaled by the free motor velocity, v_0. We assume that all overlaps between filaments are of the same length, l, and have the same density of motors, λ, and thus $F_s = \lambda l f_s$.

Three-filament clusters:

Panel a: $\tilde{v}_1 = -\tilde{v}_3 = \frac{F_s - f_{ex}}{F_s + \xi v_0}$, $\tilde{v}_2 = 0$. In the limit $\xi v_0/F_s \to 0$:, $\tilde{v}_1 = -\tilde{v}_3 = \frac{F_s - f_{ex}}{F_s}$, $v_2 = 0$.

Panel b:
$\tilde{v}_1 = -\tilde{v}_3 = -\frac{f_{ex}}{3F_s + \xi v_0}$, $\tilde{v}_2 = 0$. In the limit $\xi v_0/F_s \to 0$:, $\tilde{v}_1 = -\tilde{v}_3 = -\frac{f_{ex}}{3F_s}$, $\tilde{v}_2 = 0$.

Panel c:
$\tilde{v}_1 = -\tilde{v}_3 = \frac{2F_s - f_{ex}}{3F_s + \xi v_0}$, $\tilde{v}_2 = 0$. In the limit $\xi v_0/F_s \to 0$:, $\tilde{v}_1 = -\tilde{v}_3 = \frac{2F_s - f_{ex}}{3F_s}$, $\tilde{v}_2 = 0$.

Five-filament clusters:

Panel d:
$\tilde{v}_1 = -\tilde{v}_5 = \frac{(F_s - f_{ex})(2F_s + \xi v_0)}{F_s^2 + 3v_0 F_s + \xi^2 v_0^2}$, $\tilde{v}_2 = -\tilde{v}_4 = \frac{F_s(F_s - f_{ex})}{F_s^2 + 3v_0 F_s + \xi^2 v_0^2}$, $\tilde{v}_3 = 0$.
In the limit $\xi v_0/F_s \to 0$:, $\tilde{v}_1 = -\tilde{v}_5 = \frac{2(F_s - f_{ex})}{F_s}$, $\tilde{v}_2 = -\tilde{v}_4 = \frac{F_s - f_{ex}}{F_s}$, $\tilde{v}_3 = 0$.

Panel e:
$\tilde{v}_1 = -\tilde{v}_5 = -\frac{f_{ex}(2F_s + \xi v_0)}{5F_s^2 + 5\xi v_0 F_s + \xi^2 v_0^2}$, $\tilde{v}_2 = -\tilde{v}_4 = -\frac{F_s f_{ex}}{5F_s^2 + 5\xi v_0 F_s + \xi^2 v_0^2}$, $\tilde{v}_3 = 0$.
In the limit $\xi v_0/F_s \to 0$:, $\tilde{v}_1 = -\tilde{v}_5 = -\frac{2f_{ex}}{5F_s}$, $\tilde{v}_2 = -\tilde{v}_4 = -\frac{f_{ex}}{5F_s}$, $\tilde{v}_3 = 0$.

Panel f:
$\tilde{v}_1 = -\tilde{v}_5 = -\frac{(2F_s - f_{ex})(2F_s + \xi v_0)}{3F_s^2 - \xi v_0 F_s - \xi^2 v_0^2}$, $\tilde{v}_2 = -\tilde{v}_4 = -\frac{F_s(2F_s - f_{ex})}{3F_s^2 - \xi v_0 F_s - \xi^2 v_0^2}$, $\tilde{v}_3 = 0$.
In the limit $\xi v_0/F_s \to 0$:, $\tilde{v}_1 = -\tilde{v}_5 = -\frac{2(2F_s - f_{ex})}{3F_s}$, $\tilde{v}_2 = -\tilde{v}_4 = -\frac{2F_s - f_{ex}}{3F_s}$, $\tilde{v}_3 = 0$.

Panel g:
$\tilde{v}_1 = -\tilde{v}_5 = \frac{F_s(3F_s - 4f_{ex}) + (F_s - f_{ex})\xi v_0}{3F_s^2 + 5\xi v_0 F_s + \xi^2 v_0^2}$,
$\tilde{v}_2 = -\tilde{v}_4 = -\frac{F_s(f_{ex} + \xi v_0)}{3F_s^2 + 5\xi v_0 F_s + \xi^2 v_0^2}$, $\tilde{v}_3 = 0$.
In the limit $\xi v_0/F_s \to 0$:, $\tilde{v}_1 = -\tilde{v}_5 = \frac{3F_s - 4f_{ex}}{3F_s}$, $\tilde{v}_2 = -\tilde{v}_4 = \frac{-f_{ex}}{3F_s}$, $\tilde{v}_3 = 0$.

Panel h:
$\tilde{v}_1 = -\tilde{v}_5 = \frac{F_s(5F_s - 4f_{ex}) + (F_s - f_{ex})\xi v_0}{3F_s^2 + 5\xi v_0 F_s + \xi^2 v_0^2}$,
$\tilde{v}_2 = -\tilde{v}_4 = -\frac{F_s(2F_s - f_{ex} + \xi v_0)}{3F_s^2 + 5\xi v_0 F_s + \xi^2 v_0^2}$, $\tilde{v}_3 = 0$.
In the limit $\xi v_0/F_s \to 0$:, $\tilde{v}_1 = -\tilde{v}_5 = \frac{5F_s - 4f_{ex}}{3F_s}$, $\tilde{v}_2 = -\tilde{v}_4 = \frac{2F_s - f_{ex}}{3F_s}$, $\tilde{v}_3 = 0$.

Acknowledgements

References

1 D. Bray, *Cell movements*, Garland Science, New York, 2002.
2 T. J. Mitchison, *Philos Trans R*, 1992, **336**, 99–106.
3 M. K. Gardner, D. J. Odde and K. Bloom, *Trends Cell Biol.*, 2008, **18**, 307–310.
4 F. Bartolini and G. G. Gundersen, *J. Cell Sci.*, 2006, **119**, 4155–4163.
5 T. J. Keating and G. G. Borisy, *Biol. Cell.*, 1999, **91**, 321–329.
6 S. R. Patel, J. L. Richardson, H. Schulze, E. Kahle, N. Galjart, K. Drabek, R. A. Shivdasani, J. H. Hartwig and J. E. Italiano, *Blood*, 2005, **106**, 4076–4085.
7 K. A. Myers, Y. He, T. P. Hasaka and P. W. Baas, *Neuroscientist*, 2006, **12**, 107–118.
8 L. Ferhat, G. Rami, I. Medina, Y. Ben-Ari and A. Represa, *J. Cell Sci.*, 2001, **114**, 3899–3904.
9 L. Dehmelt, P. Nalbant, W. Steffen and S. Halpain, *Brain Cell Biol.*, 2006, **35**, 39–56.
10 P. W. Grabham, G. E. Seale, M. Bennecib, D. J. Goldberg and R. B. Vallee, *J. Neurosci.*, 2007, **27**, 5823–5834.
11 J. M. Scholey, I. Brust-Mascher and A. Mogilner, *Nature*, 2003, **422**, 746–752.
12 I. Brust-Mascher, G. Civelekoglu-Scholey, M. Kwon, A. Mogilner and J. M. Scholey, *Proc. Natl. Acad. Sci.*, 2004, **101**, 15938–15943.
13 L. C. Kapitein, E. J. Peterman, B. H. Kwok, J. H. Kim, T. M. Kapoor and C. F. Schmidt, *Nature*, 2005, **435**, 114–118.
14 G. Yang, B. R. Houghtaling, J. Gaetz, J. Z. Liu, G. Danuser and T. M. Kapoor, *Nat. Cell Biol.*, 2007, **9**, 1233–1242.
15 K. S. Burbank, T. J. Mitchison and D. S. Fisher, *Curr. Biol.*, 2007, **17**, 1373–1383.
16 D. E. Discher, P. Janmey and Y. Wang, *Science*, 2005, **310**, 1139–1143.
17 S. Kumar, I. Z. Maxwell, A. Heisterkamp, T. R. Polte, T. P. Lele, M. Salanga, E. Mazur and D. E. Ingber, *Biophys. J.*, 2006, **90**, 3762–3773.
18 T. M. Svitkina, A. b. Verkhovsky, K. M. McQuade and G. G. Borisy, *J. Cell Biol.*, 1997, **139**, 397–415.
19 D. Biron, E. Alvarez-Lacalle, T. Tlusty and E. Moses, *Phys. Rev. Lett.*, 2005, **95**, 098102.
20 A. E. Carlsson, *Phys. Rev. E*, 2006, **74**, 051912.
21 A. Zumdieck, K. Kruse, H. Bringmann, A. A. Hyman and F. Julicher, *PLoS ONE*, 2007, **2**, e696.
22 K. Kruse and F. Julicher, *Physical Review Letters*, 2000, **85**(8), 1778–1781.
23 K. Kruse, A. Zumdieck and F. Julicher, *Europhysics Letters*, 2003, **64**(5), 716–722.
24 T. B. Liverpool and M. C. Marchetti, *Phys. Rev. Let.*, 2003, **90**, 138102.
25 F. Ziebert and W. Zimmermann, *Eur. Phys. J. E*, 2005, **18**, 41–54.
26 F. Nédélec, *J. Cell Biol.*, 2002, **158**, 1005–1015.
27 J. Howard, *Mechanics of Motor Proteins and the Cytoskeleton*, Sinauer Associates, Sunderland, Massachusetts, 2001.
28 K. Tawada and K. Sekimoto, *J. Theor. Biol.*, 1991, **150**, 193–200.
29 M. T. Valentine, P. M. Fordyce, T. C. Krzysiak, S. P. Gilbert and S. M. Block, *Nat. Cell Biol.*, 2006, **8**, 470–476.
30 R. Mallik, B. C. Carter, S. A. Lex, S. J. King and S. P. Gross, *Nature*, 2004, **427**, 649–652.
31 S. Klumpp and R. Lipowsky, *Proc. Natl. Acad. Sci. USA*, 2005, **102**, 17284–17289.
32 A. Kunwar, M. Vershinin, J. Xu and S. P. Gross, *Curr. Biol.*, 2008, **18**, 1173–1183.
33 L. T. Haimo and J. L. Rosenbaum, *Cell Motil.*, 1981, **1**, 499–515.
34 L. T. Haimo and R. D. Fenton, *Cell Motil.*, 1984, **4**, 371–385.
35 A. Vilfan, E. Frey, F. Schwabl, M. Thormhlen, Y. H. Song and E. Mandelkow, *J. Mol. Biol.*, 2001, **312**, 1011–1026.
36 C. J. Sciambi, D. J. Komma, H. N. Skold, K. Hirose and S. A. Endow, *Traffic*, 2005, **6**, 1036–1046.
37 D. Stauffer and A. Aharony, *Introduction to Percolation Theory*, Taylor and Francis, London, 2nd edn, 1992.
38 N. G. Kampen, *Stochastic Processes in Physics and Chemistry*, North Holland, 3rd edn, 2007.
39 A. J. Bray, *Adv. Phys.*, 1994, **43**, 357–459.
40 P. W. Baas, J. S. Deitch, M. M. Black and G. A. Banker, *Proc. Natl. Acad. Sci.*, 1988, **85**, 8335–8339.
41 S. Patel-Hett, J. L. Richardson, H. Schulze, K. Drabek, N. A. Isaac, K. Hoffmeister, R. A. Shivdasani, J. C. Bulinski, N. Galjart, J. H. Hartwig and J. E. Italiano, *Blood*, 2008, **111**, 4605–4616.
42 D. K. Cheerambathur, G. Civelekoglu-Scholey, I. Brust-Mascher, P. Sommi, A. Mogilner and J. M. Scholey, *J. Cell Biol.*, 2007, **177**, 995–1004.

This journal is © the Owner Societies 2009

Phys. Chem. Chem. Phys., 2009, **11**, 4821–4833 | 4833